RAA 2021 Vol. **21** No. **12**, 305(8pp) doi: 10.1088/1674-4527/21/12/305

http://www.raa-journal.org *http://iopscience.iop.org/raa*

***R**esearch in*
***A**stronomy and*
***A**strophysics*

Hadronuclear interpretation of the possible neutrino emission from PKS B1424-418, GB6 J1040+0617 and PKS 1502+106

Ze-Rui Wang[2] and Rui Xue[1⋆]

[1] Department of Physics, Zhejiang Normal University, Jinhua 321004, China; *ruixue@zjnu.edu.cn*
[2] College of Physics and Electronic Engineering, Qilu Normal University, Jinan 250200, China

Received 2021 June 2; accepted 2021 September 27

Abstract In addition to neutrino event IceCube-170922A which is observed to be associated with a γ-ray flare from blazar TXS 0506+056, there are also several neutrino events that may be associated with blazars. Among them, PKS B1424-418, GB6 J1040+0617 and PKS 1502+106 are low synchrotron peaked sources, which are usually believed to have the broad line region in the vicinity of the central black hole. They are considered as counterparts of IceCube event 35, IceCube-141209A and IceCube-190730A, respectively. By considering the proton-proton (pp) interactions between the dense gas clouds in the broad line region and the relativistic protons in the jet, we show that the pp model that is applied in this work can not only reproduce the multi-waveband spectral energy distribution but also suggest a considerable annual neutrino detection rate. We also discuss the emission from the photopion production and Bethe-Heitler pair production with a sub-Eddington jet power that is suggested in our model and find that it has little effect on the spectrum of total emission for all of three sources.

Key words: neutrinos — galaxies: active — galaxies: jets — radiation mechanisms: non-thermal

1 INTRODUCTION

Blazars are a special class of active galactic nuclei (AGNs), with relativistic jets pointing nearly towards the observer (Urry & Padovani 1995). On 2017 September 22, a 290 TeV neutrino (IceCube-170922A) was detected by IceCube Observatory (IceCube Collaboration et al. 2018). This neutrino event is seen as the first time coinciding spatially and temporally with a γ-ray flare from the blazar TXS 0506+056, with a significance of $\sim 3\sigma$. This event has been studied in detail by the photohadronic interaction model ($p\gamma$ model; Gao et al. 2019; Keivani et al. 2018; Cerruti et al. 2019; Xue et al. 2019a) and hadronuclear interaction model (pp model; Liu et al. 2019).

In addition to IceCube-170922A, several other neutrino events may also be associated with blazars. Among them, three sources are low synchrotron peaked (LSP; Abdo et al. 2010) objects. One is the third PeV neutrino event, named IceCube event 35 or "Big Bird". A positional and temporal coincidence between this cascade-like 2 PeV neutrino event and a major γ-ray outburst of FSRQ PKS B1424-418 with a redshift of $z = 1.522$ is reported in Kadler et al. (2016), while the chance coincidence is about 5% (i.e., a 2σ confidence level correlation). The energy output from the outburst of PKS B1424-418 is high enough to explain this 2 PeV event, which suggests a direct physical association. Gao et al. (2017) has studied the multi-waveband emission and neutrino detection rate of PKS B1424-418 with a conventional one-zone $p\gamma$ model carefully and comprehensively. With analytical and semi-analytical methods, they demonstrate that only a lepto-hadronic model which is dominated by leptonic emission can explain the multi-waveband emission of PKS B1424-418. In the modeling of Gao et al. (2017), because the derived blob radius (7.5×10^{17} cm) is very large, they suggest that the blob is far away from the central black hole which implies that the external-Compton (EC) emission, in which soft photons are from external photon fields in the inverse Compton (IC) scattering, is weak enough to be ignored, thus the synchrotron-self Compton (SSC) emission, in which soft photons are mainly from the synchrotron photon field emitted by the same population of electrons, is dominant in the GeV band. Note that the hadronic emission is not indispensable in reproducing the spectral energy distribution (SED) of PKS B1424-418. Its SEDs on 2013 April 2 and 29 have been fitted well by a pure leptonic EC model (Tavecchio et al. 2013). After assuming the relativistic protons are injected into the blob with a super-Eddington power, Gao et al. (2017)

⋆ Corresponding author

suggest that about 0.3 neutrino event may coincide with the outburst of PKS B1424-418. Recently, GB6 J1040+0617 has been considered as another potential γ-ray counterpart for the HESE 97.4 TeV neutrino event IceCube-141209A (Garrappa et al. 2019; Kopper & IceCube Collaboration 2017; IceCube Collaboration et al. 2018). Within the 90% error region of IceCube-141209A, Garrappa et al. (2019) identify that GB6 J1040+0617 is the only cataloged gamma-ray source, which is located at a distance of $0.^{\circ}70$ from the best-fit neutrino position. GB6 J1040+0617 is an LSP BL Lac object, located at $z = 0.7351$. Its γ-ray flare and strong optical activity coincide with the detection of IceCube-141209A. The probability of finding an unassociated brighter source within the error circle is $p = 1\%$, which corresponds to a Gaussian equivalent one-sided probability of 2.3σ (Garrappa et al. 2019). The FSRQ PKS 1502+106 is located within the 50% uncertainty region of the GOLD 300 TeV neutrino event IceCube-190730A (Kiehlmann et al. 2019). While it was found in the γ-ray band to be a low state around the neutrino arrival time, an increase of radio emission at 15 GHz for PKS 1502+106 was measured with the OVRO 40m Telescope, which peak is coincident with IceCube-190730A (Kiehlmann et al. 2019; Franckowiak et al. 2020). It is similar to the situation that occurred in the case of TXS 0506+056. Rodrigues et al. (2021) consider two one-zone hadronic models to describe the multi-wavelength emission of PKS 1502+106, a leptohadronic model of γ-ray derived from electron EC emission and a proton synchrotron model of GeV emission originated in proton synchrotron radiation. They find that the results are compatible with the detection of a neutrino. However, their results also suggest that a much higher annual neutrino detection rate in the γ-ray flaring state, which has not been discovered in the archival search of IceCube events. In addition to these three sources, there are other LSP neutrino candidates. However, other neutrino candidates do not have (quasi-) simultaneous SEDs and their chance probabilities are quite low. For example, for MG3 J225517+2409 in Franckowiak et al. (2020), it is excluded in our sample because of its large angular uncertainty (roughly $30\,\mathrm{deg}^2$ for 90 % angular uncertainty) and the chance probability to find the neutrino in a period of increased gamma-ray activity at this level or higher is only $p_\gamma = 4\%$.

Alternative to the conventional $p\gamma$ models, pp models (e.g. Araudo et al. 2010; Barkov et al. 2010; Bosch-Ramon et al. 2012; Dar & Laor 1997; Liu et al. 2019) can also reproduce the multi-waveband SED and emit neutrinos. The existence of dense material surrounding the jets makes jet-medium interactions very likely. Studies of the interaction between the BLR (broad-line region) (Dar & Laor 1997) or a red giant (Bednarek & Protheroe 1997) after entering the jet has been carried out. As we know, the detection of broad emission lines is direct evidence of presence of BLR for PKS B1424-418 and PKS 1502+106 (Urry & Padovani 1995; Madejski et al. 1999). For GB6 J1040+0617, no broad emission lines are identified (Maselli et al. 2015). Whereas, because GB6 J1040+0617 is an LSP object, the requirement of EC component for fitting the high-energy component can also be seen as circumstantial evidence of presence of BLR (Böttcher & Bloom 2000; Böttcher 2007), which might be outshone by the luminous jet emission (Giommi et al. 2013). Therefore, we can still assume the existence of BLR for GB6 J1040+0617. If the energy dissipation of relativistic protons takes place in the BLR, the dense gas clouds can provide a considerable pp interaction efficiency. Such a pp interaction efficiency is not directly related to the opacity of internal $\gamma\gamma$ pair production, thus imply a possible solution to fit the SED and provide a high neutrino detection rate with a sub-Eddington jet power (Xue et al. 2019b). In this paper, the pp model developed by Liu et al. (2019) is applied to study the multi-waveband emission and neutrino flux of PKS B1424-418, GB6 J1040+0617 and PKS 1502+106.

The rest of this paper is structured as follows. In Section 2 we present the model description. We apply the pp model to PKS B1424-418, GB6 J1040+0617 and PKS 1502+106 in Section 3; in Section 4 we present our discussion and conclusions. Throughout the paper, the ΛCDM cosmology with $H_0 = 70\,\mathrm{km\,s^{-1}Mpc^{-1}}$, $\Omega_\mathrm{m} = 0.3$, $\Omega_\Lambda = 0.7$ is adopted.

2 MODEL DESCRIPTION

It is necessary to consider the hadronic processes to explain the detection of high energy neutrinos. To explain the full-wave band SED and give a sufficient neutrino production rate simultaneously, we invoke the "inner–outer blob model" (Liu et al. 2019; Xue et al. 2019a, 2021): (i) a dissipation region in the BLR (hereafter referred to as inner blob), in which the emission is mainly from the pp interaction and the secondary cascades, and (ii) a second dissipation region beyond the BLR (hereafter referred to as outer blob), in which the emission is originated from relativistic electrons. In the model we basically follow the approach of Liu et al. (2019). The model is detailed in the following subsections. In the following, the subscript 'out' indicates this parameter belongs to the outer blob, the subscript 'in' indicates this parameter belongs to the inner blob. All parameters are measured in the jet comoving frame unless otherwise specified.

2.1 Leptonic Emission from Outer Blob Beyond the BLR

It is assumed that the relativistic particles are injected into outer blob which has a spherical geometry with a radius

$R_{\rm out}$, a uniformly entangled magnetic field $B_{\rm out}$ and a Doppler factor δ. Assuming the jet moves with a bulk Lorentz factor Γ, we have $\delta \approx \Gamma$ for a relativistic jet close to the line of sight in blazars with a viewing angle of $\theta \lesssim 1/\Gamma$. Because of the low particle density and low soft photon density in outer blob, hadronic emission (i.e., pp interaction and $p\gamma$ interaction) could be neglected reasonably.

Relativistic electrons are assumed to be injected in outer blob with a broken power law distribution (Ghisellini et al. 2010), i.e.,

$$Q_{\rm e}(\gamma_{\rm e}) = Q_{\rm e,0}\gamma_{\rm e}^{-n_{\rm e,1}}\left[1+\left(\frac{\gamma_{\rm e}}{\gamma_{\rm e,b}}\right)^{(n_{\rm e,2}-n_{\rm e,1})}\right]^{-1}, \quad (1)$$
$$\gamma_{\rm e,min} < \gamma_{\rm e} < \gamma_{\rm e,max},$$

where $Q_{\rm e,0}$ is the normalization, $\gamma_{\rm e,b}$ is the break electron Lorentz factor, $n_{\rm e,1}$ and $n_{\rm e,2}$ represent the spectral indices below and above $\gamma_{\rm e,b}$, $\gamma_{\rm e,min}$ and $\gamma_{\rm e,max}$ are the minimum and maximum electron Lorentz factors. After giving an electron injection luminosity, $Q_{\rm e,0}$ can be obtained from $\int Q_{\rm e}\gamma_{\rm e}m_{\rm e}c^2 d\gamma_{\rm e} = L_{\rm e,inj}/(4/3\pi R_{\rm out}^3)$ where $m_{\rm e}$ is the electron rest mass and c is the speed of light. The steady-state electron distribution can be approximated as

$$N_{\rm e}(\gamma_{\rm e}) = Q_{\rm e}(\gamma_{\rm e})t_{\rm e}, \quad (2)$$

where $t_{\rm e} = \min\{t_{\rm cool}, t_{\rm e,dyn}\}$. $t_{\rm cool} = \frac{3m_{\rm e}c}{4(U_{\rm B}+\kappa_{\rm KN}U_{\rm ph})\sigma_{\rm T}\gamma_{\rm e}}$ is the electron radiative cooling timescale where $U_{\rm B} = \frac{B_{\rm out}^2}{8\pi}$ is the energy density of the magnetic field, $U_{\rm ph}$ is the energy density of the soft photons, $\sigma_{\rm T}$ is the Thomson scattering cross section and $\kappa_{\rm KN}$ is a numerical factor accounting for the Klein-Nishina effect (Moderski et al. 2005). $t_{\rm e,dyn} = \frac{R_{\rm out}}{c}$ is the dynamical timescale of outer blob. Based on $N_{\rm e}(\gamma_{\rm e})$, the synchrotron and synchrotron self-Compton (SSC) emission can be calculated (Katarzyński et al. 2001).

In the external Compton (EC) mechanism, the contributions of BLR and dust torus (DT) emission are considered (e.g., Tan et al. 2020). The energy density of BLR ($u_{\rm BLR}$) and dust torus ($u_{\rm DT}$) emission as a function of the distance r between the central black hole and the dissipation region can be approximated by (Hayashida et al. 2012)

$$u_{\rm BLR} = \frac{\eta_{\rm BLR}\Gamma^2 L_{\rm d}}{3\pi r_{\rm BLR}^2 c[1+(r/r_{\rm BLR})^3]} \quad (3)$$

and

$$u_{\rm DT} = \frac{\eta_{\rm DT}\Gamma^2 L_{\rm d}}{3\pi r_{\rm DT}^2 c[1+(r/r_{\rm DT})^4]}, \quad (4)$$

where $\eta_{\rm BLR} = 0.1$ and $\eta_{\rm DT} = 0.1$ are the fractions of the disk luminosity $L_{\rm d}$ reprocessed into BLR and dust torus radiation, respectively, $r_{\rm BLR} = 0.1(L_{\rm d}/10^{46}{\rm ergs}^{-1})^{1/2}$pc and $r_{\rm DT} = 2.5(L_{\rm d}/10^{46}{\rm ergs}^{-1})^{1/2}$pc are the characteristic distances where the above reprocessing takes place. The BLR and DT radiation is taken as an isotropic blackbody with a peak at $\approx 2.82k_{\rm B}T\Gamma/h \approx 2\times10^{15}\Gamma$ Hz (Tavecchio & Ghisellini 2008) and $3\times10^{13}\Gamma$ Hz (Cleary et al. 2007) in the jet comoving frame, respectively, where T is the corresponding characteristic temperature of BLR or DT. The correlations between $u_{\rm BLR}$, $u_{\rm DT}$ and r are shown in Figure 1. In the EC process, the EC process is named EC/BLR if the energy density of the BLR dominates, otherwise it is named EC/DT.

2.2 Hadronic Emission from Inner Blob in the BLR

Similar to outer blob, inner blob also has a spherical geometry with the same Doppler factor δ, but with different radius $R_{\rm in}$ and magnetic field $B_{\rm in}$. Assuming that the inner blob is filled with the BLR clouds, a considerable pp interaction efficiency can be obtained if one takes the typical hydrogen column density of BLR clouds as $N_{\rm H} \approx 10^{23}{\rm cm}^{-2}$ (Peterson 2006).

Relativistic protons are assumed to be injected in inner blob with a power-law distribution, i.e.,

$$Q_{\rm p}(\gamma_{\rm p}) = Q_{\rm p,0}\gamma_{\rm p}^{-n_{\rm p}}, \gamma_{\rm p,min} < \gamma_{\rm p} < \gamma_{\rm p,max}, \quad (5)$$

where $Q_{\rm p,0}$ is the normalization, $n_{\rm p}$ is the spectral index, and $\gamma_{\rm p,min}$ and $\gamma_{\rm p,max}$ are the minimum and maximum proton Lorentz factors. As we described in Section 2.1, $Q_{\rm p,0}$ can be obtained by giving a proton injection luminosity $L_{\rm p,inj}$ in the same way. Also, the steady-state proton distribution can be approximated as

$$N_{\rm p}(\gamma_{\rm p}) = Q_{\rm p}(\gamma_{\rm p})t_{\rm p}, \quad (6)$$

where $t_{\rm p} = \min\{t_{\rm pp}, t_{\rm p,dyn}\}$. More specifically, $t_{\rm pp} = \frac{R_{\rm in}}{\kappa\sigma_{\rm pp}cN_{\rm H}}$ is the pp interaction cooling timescale, where $\kappa \approx 0.5$ is the inelasticity of the pp interaction and the corresponding cross section $\sigma_{\rm pp}$ can be approximated as in Kelner et al. (2006), and $t_{\rm p,dyn} = \frac{R_{\rm in}}{c}$ is the dynamical timescale of the inner blob.

The secondary π^0 and $\pi^\pm$ that generated through the pp interaction are short-lived and finally decayed into γ-ray photons, electrons/positrons and neutrinos, i.e.,

$$p+p \rightarrow \pi^0 \rightarrow \gamma+\gamma,$$
$$p+p \rightarrow \pi^+ \rightarrow \nu_\mu+\mu^+ \rightarrow \nu_\mu+e^++\nu_{\rm e}+\bar{\nu}_\mu,$$
$$p+p \rightarrow \pi^- \rightarrow \bar{\nu}_\mu+\mu^- \rightarrow \bar{\nu}_\mu+e^-+\bar{\nu}_{\rm e}+\nu_\mu.$$

With the above steady-state proton distribution $N_{\rm p}(\gamma_{\rm p})$, the differential spectrum of decayed γ-ray photons, electrons/positrons and neutrinos can be calculated with simple analytical expressions that developed by Kelner et al. (2006).

The energy distribution of ultra-high-energy (UHE) γ-ray induced pair cascades is evaluated using a semianalytical method that developed by Böttcher et al. (2013). The absorbed UHE photons will be redistributed at lower

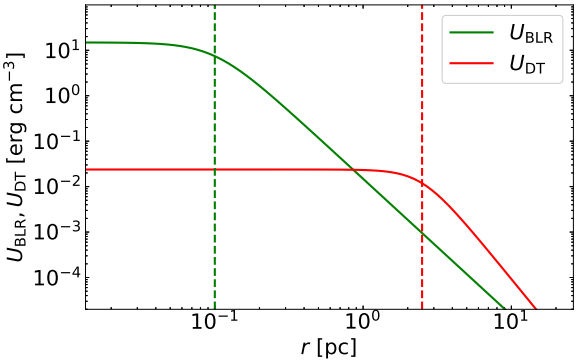

Fig. 1 Energy densities as a function of the distance r between the central black hole and the dissipation region with $\Gamma = 20$ and $L_{\rm d} = 10^{46}$ erg s^{-1}. The *green* and *red solid lines* represent $u_{\rm BLR}$ and $u_{\rm DT}$, respectively. The *green* and *red dashed vertical lines* represent $r_{\rm BLR}$ and $r_{\rm DT}$, respectively.

energies through synchrotron, SSC and EC emission from pair cascades. In $p\gamma$ models, many recent studies (Gao et al. 2019; Keivani et al. 2018; Cerruti et al. 2019; Xue et al. 2019a) suggest that the synchrotron X-ray emission from pair cascades will overshoot the observation data easily which implies a low neutrino flux. However, such an issue can be improved in BLR because of the large Compton opacity for photons with its energy less than MeV. Photons emitted by pair cascades can ionize the BLR. UV and X-ray photons will be scattered by ionized electrons in another direction from the line of sight. The optical depth is $\tau_{\rm sc} = \sigma_{\rm sc} N_{\rm H}$ where

$$\sigma_{\rm sc} = \frac{3}{4}\sigma_{\rm T}\left(\frac{1+x}{x^3}\left[\frac{2x(1+x)}{1+2x} - \ln(1+2{\rm x})\right] + \frac{1}{2x}\ln(1+2x) - \frac{1+3x}{(1+2x)^2}\right) \quad (7)$$

with $x = E/m_{\rm e}c^2$ and E represent the photon energy. This absorption will modify the emission in BLR by the factor $(1-{\rm e}^{-\tau_{\rm sc}})/\tau_{\rm sc}$. With $N_{\rm H}$ given in Table 1, it can be seen that the optical depth $\tau_{\rm sc}$ is equal to unity around 1 keV for three objects.

In addition to the hadronic emission, the primary electrons in the inner blob may also contribute considerable radiation in the GeV band. However, its contribution is not essential to the fitting of SED, and can even be a sub-dominant component by adjusting the parameters[1]. Therefore, in order to reduce the unnecessary free parameters as many as possible, we neglect the leptonic emission from the inner blob in the modeling.

Finally, the very high energy (VHE) γ-ray photons that can escape from inner and outer blobs will be absorbed

[1] Emissions derived from primary electrons in the inner blob may be the reason for the association between neutrino events and photon emission flares. However, it will invoke more parameters if we take this into account, then the fitting becomes fine-tuning parameters.

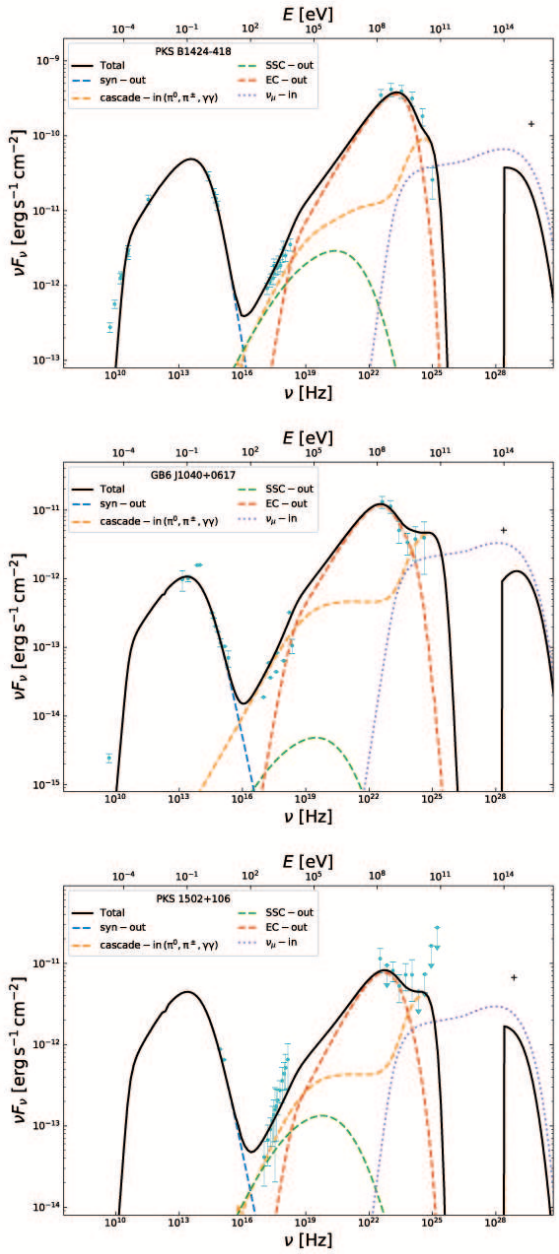

Fig. 2 The pp model for modeling of PKS B1424-418 (*upper panel*), GB6 J1040+0617 (*middle panel*) and PKS 1502+106 (*bottom panel*). The (quasi-) simultaneous SED of PKS B1424-418 is taken from Gao et al. (2017). While the multi-wavelength SED of GB6 J1040+0617 is not contemporaneous, which is taken from Garrappa et al. (2019). The simultaneous SED of PKS 1502+106 is taken from Franckowiak et al. (2020). The *blue*, *green* and *red dashed curves* represent the synchrotron, SSC and EC emission from relativistic electrons in the outer blob, respectively. The *orange dashed curves* represent the emission from cascade pairs and decayed γ-ray. The *purple dotted curve* is the neutrino spectrum. The *black solid curve* is the total emission from the inner and outer blobs. The *black cross* represents the neutrino flux on the corresponding energy (2 PeV for PKS B1424-148, 97.4 TeV for GB6 J1040+0617 and 300 TeV for PKS 1502+106) during 1 year observation.

by the extragalactic background light (EBL). It makes the observed spectrum in the VHE band steeper than the intrinsic one. According to the EBL model (model C) presented by Finke et al. (2010), we calculate the absorption in the GeV-TeV band.

3 APPLICATIONS

3.1 Parameters Constraints

After considering the leptonic and hadronic emission from two dissipation regions, there are 19 free parameters in our model: eight for the two dissipation regions (δ, $B_{\rm in}$, $B_{\rm out}$, $R_{\rm in}$, $R_{\rm out}$, $r_{\rm in}$, $r_{\rm out}$ and $L_{\rm d}$), six for the injected primary relativistic electrons in outer blob ($L_{\rm e,inj}$, $n_{\rm e,1}$, $n_{\rm e,2}$, $\gamma_{\rm e,min}$, $\gamma_{\rm e,b}$ and $\gamma_{\rm e,max}$) and five for the injected relativistic protons in inner blob ($L_{\rm p,inj}$, $n_{\rm p}$, $\gamma_{\rm p,min}$, $\gamma_{\rm p,max}$ and $N_{\rm H}$). Our strategies for reducing the parameter space are as follows.

1. As mentioned in Section 2.2, inner blob is located in the BLR, therefore $r_{\rm in}$ is set to 0.1 pc, which is the characteristic distance of BLR. But $r_{\rm out}$ has to be a free parameter which can be constrained by fitting the GeV data.

2. We set the disk luminosities $L_{\rm d}$ of PKS B1424-418 and PKS 1502+106 are both 10^{46} erg s^{-1} as inferred in Tavecchio et al. (2013) and Ding et al. (2019), respectively. For GB6 J1040+0617, its disk luminosity is assumed to be the same value.

3. Assuming that the injection electrons and protons are accelerated with the diffusive shock acceleration mechanism, $n_{\rm e,1} = n_{\rm p} = 2$ (Drury 1983; Bednarz & Ostrowski 1998) is adopted in our modeling.

4. In leptonic models, the minimum electron Lorentz factor $\gamma_{\rm e,min}$ is constrained by the hard X-ray data which is explained by the low-energy tail of SSC emission (Celotti & Ghisellini 2008; Madejski et al. 2016). However, in hadronic models, the synchrotron emission from pair cascades will have a significant contribution to the hard X-ray band. Therefore, $\gamma_{\rm e,min}$ cannot be constrained by fitting SED. In our calculation, the typical value $\gamma_{\rm e,min} = 50$ is adopted.

5. We set the maximum electron Lorentz factor $\gamma_{\rm e,max} = 10^7$, because its impact on our model is minor.

6. The minimum proton Lorentz factor $\gamma_{\rm p,min} = 1$ is adopted, which will not affect our fitting results.

7. Generally, $\gamma_{\rm p,max}$ can be obtained when the acceleration timescale is equal to the escape timescale, which is assumed to be equal to the dynamical timescale $t_{\rm p,dyn}$. If one assumes that diffusive shock acceleration is the dominant acceleration mechanism, the acceleration timescale can be evaluated by (Protheroe & Clay 2004; Rieger et al. 2007)

$$t_{\rm acc} \simeq \frac{20\alpha}{3}\frac{r_{\rm L}}{c} \simeq \frac{20\alpha}{3}\frac{\gamma_{\rm p} m_{\rm p} c}{eB_{\rm II}}, \tag{8}$$

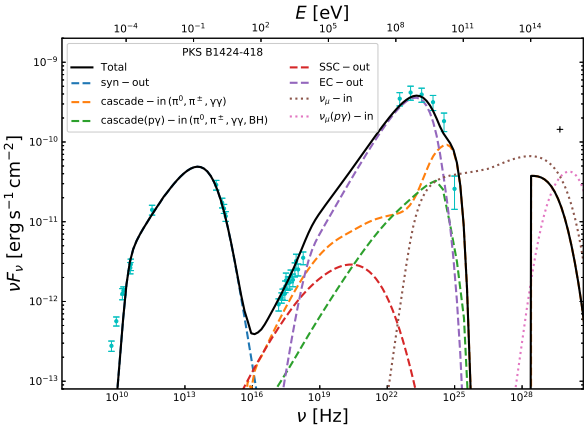

Fig. 3 The SED of PKS B1424-418 when considering the photopion production and Bethe-Heitler (BH) process in the inner blob. The *green dashed curve* shows the emission from decayed γ-ray in photopion production, synchrotron and IC emission from pairs produced in BH process and cascade emission in the inner blob. The *pink dotted curve* shows the spectrum of neutrinos generated in the photopion production, which peaked at $\sim$5 PeV.

where $r_{\rm L}$ is the Larmor radius of the proton and α is the parameter which in the case of shock acceleration depends on the spectrum of magnetic turbulence and on the velocity of the upstream-flow (Sikora 2011). $\alpha = 10$ for mildly relativistic shocks is adopted in our model (Lagage & Cesarsky 1983). Then $\gamma_{p,\rm max}$ can be approximated as

$$\begin{aligned}\gamma_{\rm p,max} &= \frac{3}{20}\frac{eB_{\rm in}R_{\rm in}}{\alpha m_p c^2} \\ &\simeq 5\times10^7\left(\frac{\alpha}{10}\right)^{-1}\left(\frac{B_{\rm in}}{1{\rm G}}\right)\left(\frac{R_{\rm in}}{10^{16}{\rm cm}}\right).\end{aligned} \tag{9}$$

Then the number of free parameters is reduced to 11: δ, $B_{\rm out}$, $B_{\rm in}$, $R_{\rm out}$, $R_{\rm in}$, $L_{\rm e,inj}$, n_2, $\gamma_{\rm e,b}$, $r_{\rm out}$, $L_{\rm p,inj}$ and $N_{\rm H}$. Based on the above constraints, we calculate the multiwavelength electromagnetic and neutrino emission, and the corresponding chi-square value $\chi^2 = \frac{1}{m-dof}\sum_{i=1}^{m}(\frac{\hat{y}_i - y_i}{\sigma_i})^2$, where m is the number of quasi-simultaneous observational data points, dof is the degrees of freedom, $\hat{y}_i$ is the expected values from the model, y_i is the observed data and σ_i is the standard deviation for each data point.

3.2 Modeling the SED and Neutrino Spectrum of PKS B1424-418, GB6 J1040+0617 and PKS 1502+106

After reducing the parameter space, the inner-outer blob model with pp interaction that described in Section 2 is used to explain the multi-waveband emission and neutrino flux from PKS B1424-418, GB6 J1040+0617 and PKS 1502+106. The fitting results are shown in Figure 2,

and the input model parameters are shown in Table 1. It can be seen that the hard X-ray data is dominated by the synchrotron emission from pair cascades because of requiring a high model predicted neutrino flux. Although, in the pure leptonic model, the hard X-ray observation data is explained by the SSC emission. It should be noted that the hard X-ray spectrum of PKS 1502+106 can hardly be reproduced with cascade emission solely, unless freeing the electron spectrum index $n_{\rm e,1}$, and introducing a softer one. In addition to the limit from hard X-ray data, the sub-TeV data will also put a strict limit on the contribution of pp interaction to neutrino flux. Because the neutrino spectrum is closely related to the decayed γ-ray spectrum, and the decayed γ-ray photons will contribute significant emission in the sub-TeV band in the modeling with relative high neutrino flux. So one should reduce the contribution of primary electrons emission in the sub-TeV band as much as possible. In the EC/BLR process, if one take $\gamma_{\rm e,b} = 3 \times 10^3$ and $\delta = 30$, its spectrum in observer's frame is peaked around the sub-TeV band ($\nu_{\rm EC,BLR} \approx \delta^2 \gamma_{\rm e,b}^2 2 \times 10^{15}{\rm Hz} \approx 1.62 \times 10^{25}{\rm Hz}$). In the EC/DT process, the peak frequency is around GeV band ($\nu_{\rm EC,DT} \approx \delta^2 \gamma_{\rm e,b}^2 3 \times 10^{13}{\rm Hz} \approx 2.43 \times 10^{23}{\rm Hz}$). As shown in Figure 1, the external photon field energy density of DT will exceed that of BLR if the distance r beyond about 1 pc, then the EC/DT process will dominate the emission of primary electrons in γ-ray band and the emission from the EC/BLR process will be suppressed. Therefore, if a relative high neutrino flux is required, the location of outer blob $r_{\rm out}$ should be far away from the central black hole.

The kinetic power of relativistic electrons and protons, and the power carried in the magnetic field for the parameter sets of each source are also presented in Table 1. The kinetic power in relativistic electrons in the AGN frame can be estimated as

$$P_{\rm e,k} = \pi R_{\rm out}^2 \Gamma^2 c m_{\rm e} c^2 \int d\gamma_{\rm e} N_{\rm e}(\gamma_{\rm e}) \gamma_{\rm e} \,, \qquad (10)$$

the kinetic power in relativistic protons in the AGN frame can be estimated as

$$P_{\rm p,k} = \pi R_{\rm in}^2 \Gamma^2 c m_{\rm p} c^2 \int d\gamma_{\rm p} N_{\rm p}(\gamma_{\rm p}) \gamma_{\rm p} \,, \qquad (11)$$

and the power carried in the magnetic field can be estimated as

$$P_{\rm B}^{\rm out/in} = \pi R^2 \Gamma^2 c \frac{B_{\rm out/in}^2}{8\pi}. \qquad (12)$$

The total jet power of the two dissipation regions is evaluated as $P_{\rm tot} = P_{\rm e,k} + P_{\rm p,k} + P_{\rm B}^{\rm out/in}$. Our results suggest that a sub-Eddington jet power is required in the pp model if one considers that their black hole masses are all $4.4 \times 10^9\, M_\odot$ (the Eddington luminosity is estimated as $L_{\rm Edd} = 1.26 \times 10^{38} (\frac{M}{M_\odot})$ erg s^{-1}$\approx 5.54 \times 10^{47}$ erg s^{-1}) PKS 1502+106 (Sbarrato et al. 2012). For PKS B1424-418 and GB6 J1040+0617, their black hole masses are not given in literature.

Comparing to the annual neutrino flux calculated with the effective area of IceCube's HESE event alert system (Kadler et al. 2016; Gao et al. 2017), our results suggest that the annual neutrino detection rate of PKS B1424-418 is $\sim 0.26\ {\rm yr}^{-1}$ at 2 PeV, which is similar to that in Gao et al. (2017) ($\sim 0.23\ {\rm yr}^{-1}$). Similarly, following the annual neutrino flux calculated with the IceCube point-source effective area (Garrappa et al. 2019), our predicted annual neutrino detection rate of GB6 J1040+0617 is $\sim 0.64\ {\rm yr}^{-1}$ at 97.4 TeV. The IceCube point-source effective area for (anti)muon neutrino (Carver 2019) in the decl. $-5^\circ - 30^\circ$ is employed for PKS 1502+106 to calculate the expected neutrino flux at 300 TeV ($\sim 6.68 \times 10^{-12}\ {\rm erg\,s^{-1}\,cm^{-2}}$). Then the annual neutrino detection rate of PKS 1502+106 is $\sim 0.35\ {\rm yr}^{-1}$ in our modeling which is much higher than that in Rodrigues et al. (2021) ($\sim 0.02\ {\rm yr}^{-1}$ at 300 TeV). Note that the hydrogen column density in our model is already high enough and the jet power for PKS B1424-418 is close to the Eddington luminosity ($P_{\rm tot}/L_{\rm Edd} \approx 57\%$). There is no other way to increase the neutrino flux, thus we suggest that $\sim 0.26\ {\rm yr}^{-1}$ can be seen as an upper limit of the neutrino detection rate of PKS B1424-418. While the jet powers are only 2% of the Eddington luminosity for GB6 J1040+0617 and 11% of the Eddington luminosity for PKS 1502+106, therefore their annual detection rates still have a lot of space to improve.

4 DISCUSSION AND CONCLUSIONS

4.1 $p\gamma$ Interactions in Inner and Puter Blobs

Since LSPs usually are observed with broad emission lines or seem to require an EC component to explain their GeV spectra (Böttcher & Bloom 2000; Böttcher 2007; Madejski et al. 1999), the number density of external photon fields could be so high that make the $p\gamma$ interactions efficient. Thus it is necessary to check whether the $p\gamma$ interactions will contribute significant electromagnetic and neutrino emission under the parameter sets obtained in our model.

The condition where cross section of photopion production peaks due to the $\Delta^+(1232)$ resonance is (Waxman & Bahcall 1997)

$$E_{\rm p} E_{\rm soft} \simeq 0.3\ {\rm GeV}^2, \qquad (13)$$

where $E_{\rm p}$ and $E_{\rm soft}$ are the proton and soft photon energy in the comving frame, respectively. In $p\gamma$ interactions, the neutrino energy is about 5% that of the parent proton. For PKS B1424-418, its observed neutrino energy is 2 PeV, thus its parent proton energy in the comving frame is $E_{\rm p} = 40/\delta$ PeV, where δ is 35 as given in Table 1.

Table 1 Model Parameters for SED Fitting

	PKS B1424-418	GB6 J1040+0617	PKS 1502+106
δ	35	28	35
parameters in the outer blob			
$B_{\rm out}$ [G]	0.08	0.29	0.20
$R_{\rm out}$ [cm]	9×10^{17}	9×10^{16}	2×10^{17}
$L_{\rm e,inj}$ [erg s^{-1}]	2.5×10^{43}	2.1×10^{41}	3.0×10^{42}
n_2	5.6	5.0	4.6
$\gamma_{\rm e,b}$	6×10^{3}	2×10^{3}	3×10^{3}
$r_{\rm out}$ [pc]	5.5	1.0	5.0
parameters in the inner blob			
$B_{\rm in}$ [G]	0.1	0.1	0.1
$R_{\rm in}$ [cm]	1.2×10^{16}	5.0×10^{15}	5.0×10^{15}
$L_{\rm p,inj}$ [erg s^{-1}]	4×10^{44}	2×10^{43}	7×10^{43}
$N_{\rm H}$[cm^{-2}]	3.6×10^{24}	1.5×10^{24}	1.5×10^{24}
neutrino flux on 2 PeV, 97.3 TeV and 300 TeV			
N_ν[erg cm^{-2} s^{-1}]	3.79×10^{-11}	3.26×10^{-12}	2.35×10^{-12}
kinetic power in the outer blob			
$P_{\rm e,k}$ [erg s^{-1}]	1.47×10^{46}	1.25×10^{44}	2.48×10^{45}
$P_{\rm B}$ [erg s^{-1}]	2.38×10^{46}	2.00×10^{45}	7.34×10^{45}
kinetic power in the inner blob			
$P_{\rm p,k}$ [erg s^{-1}]	3.20×10^{47}	1.07×10^{46}	5.86×10^{46}
$P_{\rm B}$ [erg s^{-1}]	6.61×10^{42}	7.34×10^{41}	1.15×10^{42}
total jet power			
$P_{\rm tot}$ [erg s^{-1}]	3.59×10^{47}	1.28×10^{46}	6.84×10^{46}
χ^2	8.1	35.4[a]	16.2

Notes: [a] The X-ray data of GB6 J1040+0617 are not (quasi-) simultaneously observed and show two distinct states. In the calculation of its χ^2, we neglect the low-state X-ray data.

Therefore, it can be seen that soft photons with energy ≈ 0.26 keV in the comoving frame are mainly collided in photopion production. Similarly, the photopion production of GB6 J1040+0617 mainly occurs with soft photons with energy $\approx$ 4.31 keV, and the soft photon energy is about 1.75 keV for PKS 1502+106. The peak energies of BLR and DT in the comoving frame are $0.25\delta_{30}$ keV and $3.72\delta_{30}$ eV, respectively, where $\delta_{30} = \delta/30$. It can be found that the soft photon energy required in the photopion production of PKS B1424-418 is close to the peak energy of the BLR, which may suggest a possible high photopion production efficiency $f_{p\gamma}$. While due to the absence of soft photons with energy around 4.31 keV for GB6 J1040+0617 or 1.75 keV for PKS 1502+106, the photopion productions of these two sources can be ignored in our modeling. Therefore, we will discuss the $p\gamma$ interactions of PKS B1424-418 in the following. The photopion production efficiency $f_{p\gamma}$ can be estimated as

$$f_{p\gamma} = Rn_{\rm soft}\left\langle\sigma_{p\gamma}\kappa\right\rangle , \quad (14)$$

where R is radius of dissipation region, $n_{\rm soft}$ is the number density of the photons, and $\langle\sigma_{p\gamma}\kappa\rangle \simeq 10^{-28}{\rm cm}^2$ is the photopion cross section weighted by inelasticity. Considering the parameters of PKS B1424-418 in Table 1, the inferred $f_{p\gamma}$ in the inner and outer blobs are 0.05 and 3.98×10^{-5}, respectively. Therefore, photopion production is inefficient in the outer blob but efficient in the inner blob.

In the following, the approach that developed by Kelner & Aharonian (2008) is employed to evaluate the $p\gamma$ interactions in the inner blob. As studied in Xue et al. (2019a), the synchrotron radiation of the primary electrons in the inner blob is suppressed by the EC/BLR emission, so that the opacity of the $\gamma\gamma$ absorption for sub-PeV/PeV gamma rays is much lower than 1. Therefore, the emission from pair cascades will not overshoot the observed X-ray emission. We present the cascade emission and the neutrino emission from $p\gamma$ interactions in Figure 3. It can be found that the emission from the pair cascades has little effect on the spectrum of total emission, especially on the hard X-ray band. Moreover, the corresponding neutrino flux that derived from $p\gamma$ interactions on 2 PeV is 3.60×10^{-12} erg cm^{-2} s^{-1} which will double the detection rate. So, in general, from our estimation and calculation above, the $p\gamma$ process will mildly affect the result of PKS B1424-418.

4.2 Conclusions

In this paper, we employ an inner-outer blob model with pp interaction developed by Liu et al. (2019) on studying the neutrino and multi-waveband emission from three potential counterparts of IceCube event 35, IceCube-141209A and IceCube-190730A. The pp model can reproduce the SEDs of PKS B1424-418, GB6 J1040+0617 and PKS 1502+106, and suggests a considerable neutrino detection rate. Whereas, because the energy dissipation of relativistic protons in the inner blob needs to occur strictly in the BLR, the dissipation probability is actually quite low (Xue et al. 2019a, 2021). Therefore, under the framework of inner-outer blob pp model, only a few blazars' energy dissipation of relativistic particles can occur in the BLR

continuously, which cannot help blazars contribute to the diffuse neutrino background significantly.

By assuming a high hydrogen column density $\sim 10^{24}\,\mathrm{cm}^{-2}$, a sub-Eddington jet power is also suggested. If we take the typical hydrogen column density of BLR clouds as $N_{\mathrm{H}} \approx 10^{23}\,\mathrm{cm}^{-2}$ (Peterson 2006), the annual neutrino detection rate of PKS B1424-418 would be much lower if the Eddington luminosity is seen as the upper limit of jet power. GB6 J1040+0617 and PKS 1502+106 can still keep the annual neutrino detection rate unchanged by increasing the jet power. Thus, the measurement of the column density in BLR is very important for the *pp* model. Moreover, since the IC emission from pair cascades and the decayed γ-ray can contribute significant emission above ~ 10 GeV, this *pp* model also has the potential to explain the hard TeV spectra of a few TeV blazars (e.g. 1ES 1101-232). In our next work, we will apply this *pp* model on some TeV blazars to reproduce their hard TeV spectra.

Acknowledgements We thank the anonymous referee for insightful comments and constructive suggestions. This work is supported by the Ph.D. Research start-up fund of Zhejiang Normal University (Grant No. YS304320082).

References

Abdo, A. A., Ackermann, M., Agudo, I., et al. 2010, ApJ, 716, 30
Araudo, A. T., Bosch-Ramon, V., & Romero, G. E. 2010, A&A, 522, A97
Barkov, M. V., Aharonian, F. A., & Bosch-Ramon, V. 2010, ApJ, 724, 1517
Bednarek, W., & Protheroe, R. J. 1997, MNRAS, 287, L9
Bednarz, J., & Ostrowski, M. 1998, Phys. Rev. Lett., 80, 3911
Bosch-Ramon, V., Perucho, M., & Barkov, M. V. 2012, A&A, 539, A69
Böttcher, M., & Bloom, S. D. 2000, AJ, 119, 469
Böttcher, M., Reimer, A., Sweeney, K., & Prakash, A. 2013, ApJ, 768, 54
Böttcher, M. 2007, Ap&SS, 309, 95
Carver, T. 2019, arXiv e-prints, arXiv:1908.05993
Celotti, A., & Ghisellini, G. 2008, MNRAS, 385, 283
Cerruti, M., Zech, A., Boisson, C., et al. 2019, MNRAS, 483, L12
Cleary, K., Lawrence, C. R., Marshall, J. A., et al. 2007, ApJ, 660, 117
Dar, A., & Laor, A. 1997, ApJL, 478, L5
Ding, N., Gu, Q. S., Geng, X. F., et al. 2019, ApJ, 881, 125
Drury, L. O. 1983, Reports on Progress in Physics, 46, 973
Finke, J. D., Razzaque, S., & Dermer, C. D. 2010, ApJ, 712, 238
Franckowiak, A., Garrappa, S., Paliya, V., et al. 2020, ApJ, 893, 162
Gao, S., Fedynitch, A., Winter, W., & Pohl, M. 2019, Nature Astronomy, 3, 88
Gao, S., Pohl, M., & Winter, W. 2017, ApJ, 843, 109
Garrappa, S., Buson, S., Franckowiak, A., Fermi-LAT Collaboration, et al. 2019, ApJ, 880, 103
Ghisellini, G., Tavecchio, F., Foschini, L., et al. 2010, MNRAS, 402, 497
Giommi, P., Padovani, P., & Polenta, G. 2013, MNRAS, 431, 1914
Hayashida, M., Madejski, G. M., Nalewajko, K., et al. 2012, ApJ, 754, 114
IceCube Collaboration, Aartsen, M. G., Ackermann, M., et al. 2018, Sci., 361, eaat1378
Kadler, M., Krauß, F., Mannheim, K., et al. 2016, Nature Physics, 12, 807
Katarzyński, K., Sol, H., & Kus, A. 2001, A&A, 367, 809
Keivani, A., Murase, K., Petropoulou, M., et al. 2018, ApJ, 864, 84
Kelner, S. R., & Aharonian, F. A. 2008, Phys. Rev. D, 78, 034013
Kelner, S. R., Aharonian, F. A., & Bugayov, V. V. 2006, Phys. Rev. D, 74, 034018
Kiehlmann, S., Hovatta, T., Kadler, M., et al. 2019, The Astronomer's Telegram, 12996
Kopper, C., & IceCube Collaboration 2017, 35th International Cosmic Ray Conference (ICRC2017), 301, 981
Lagage, P. O., & Cesarsky, C. J. 1983, A&A, 125, 249
Liu, R.-Y., Wang, K., Xue, R., et al. 2019, Phys. Rev. D, 99, 063008
Madejski, G. M., Nalewajko, K., Madsen, K. K., et al. 2016, ApJ, 831, 142
Madejski, G. M., Sikora, M., Jaffe, T., et al. 1999, ApJ, 521, 145
Maselli, A., Massaro, F., D'Abrusco, R., et al. 2015, Ap&SS, 357, 141
Moderski, R., Sikora, M., Coppi, P. S., & Aharonian, F. 2005, MNRAS, 363, 954
Peterson, B. M. 2006, in Physics of Active Galactic Nuclei at all Scales, 693, 77
Protheroe, R. J., & Clay, R. W. 2004, PASA, 21, 1
Rieger, F. M., Bosch-Ramon, V., & Duffy, P. 2007, Ap&SS, 309, 119
Rodrigues, X., Garrappa, S., Gao, S., et al. 2021, ApJ, 912, 54
Sbarrato, T., Ghisellini, G., Maraschi, L., et al. 2012, MNRAS, 421, 1764
Sikora, M. 2011, IAUS, 275, 59
Tan, C., Xue, R., Du, L.-M., et al. 2020, ApJS, 248, 27
Tavecchio, F., Pacciani, L., Donnarumma, I., et al. 2013, MNRAS, 435, L24
Tavecchio, F., & Ghisellini, G. 2008, MNRAS, 386, 945
Urry, C. M., & Padovani, P. 1995, PASP, 107, 803
Waxman, E., & Bahcall, J. 1997, Phys. Rev. Lett., 78, 2292
Xue, R., Liu, R.-Y., Wang, X.-Y., Yan, H., & Böttcher, M. 2019b, ApJ, 871, 81
Xue, R., Liu, R.-Y., Petropoulou, M., et al. 2019a, ApJ, 886, 23
Xue, R., Liu, R.-Y., Wang, Z.-R., Ding, N., & Wang, X.-Y. 2021, ApJ, 906, 51